Sea state impacts on wind speed retrievals from C-Band radars

Journal:	*Journal of Selected Topics in Applied Earth Observations and Remote Sensing*
Manuscript ID	JSTARS-2016-00504.R2
Manuscript type:	Special Issue on New Challenges and Opportunities in Scatterometry
Date Submitted by the Author:	n/a
Complete List of Authors:	Stopa, Justin; CNRS-IFREMER-IRD-UBO, Lab. of Ocean Physics and Satellite Oceanography (LOPS) MOUCHE, Alexis; CNRS-IFREMER-IRD-UBO, Lab. of Ocean Physics and Satellite Oceanography (LOPS) Chapron, Bertrand; CNRS-IFREMER-IRD-UBO, Lab. of Ocean Physics and Satellite Oceanography (LOPS) Collard, Fabrice; Ocean Data Lab, Ocean Data Lab
Keywords:	Wind, Synthetic aperture radar, Remote sensing, Surface waves, Sea surface, Microwave measurements, Satellites

Response to Associate Editor: for JSTARS-2016-00504 Sea state impacts on wind speed retrievals from C-Band radars. Our response are given below point by point.

I would just like to ask you to clean up the references list a bit, in line with the latest improvements of the paper, e.g.:
-We verified that all cited works were indeed included in the references.

- 'Shankaranarayanan and Donelan (2001)' is not listed in the references, hence referenced to in the text by the tag above and not a reference number
-We now correctly added the reference.

- In some of the references there are inverted '?' signs, which I am guessing need to be a '/' or a '.'
-I am not sure what caused that error some text interpreter error. The “<” and “>” signs were distorted in latex as a result. They are now properly displayed.

- I got a bit confused because you refer to several publications in your answer which are not listed either in the references: Piolle (2016) and Reul (2016)
-Sorry for the confusion, we did not use cite the reference Reul et al., (2016) in the main text and only used Reul et al., (2009) with reference to sea surface salinity on the NRCS.

Finally, just an editorial: in page 4 line 40 it states '! 5 m/s' and not '< 5 m/s', which I think is what you meant?
-Corrected.

I'll be happy to have a final check your updated paper. Thanks a lot in advance.
-Thank you for your attentiveness.

Sea state impacts on wind speed retrievals from C-Band radars

Justin E. Stopa, Alexis Mouche, Bertrand Chapron, and Fabrice Collard

***Abstract*—Scatterometers, a proven technology, provide ocean wind speeds and directions that are essential in operational forecasts, monitoring of the climate, and scientific applications. While the missions and geophysical model functions are performing well, challenges remain. We analyze data from Advanced SCATterometer (ASCAT) aboard MetOp-A and the Advanced Synthetic Aperture Radar (ASAR) aboard Envisat, which both operate in the C-Band, against in-situ buoy wind speeds. We observe large variability in the wind speed residuals. Through analysis of these residuals we find that they are related to sea state effects and atmospheric stability. The sea state dependence created by low frequency swells is more pronounced for the lower incidence angles in ASCAT. In ASAR with a fixed angle of 23°, the sea state dominates the wind speed errors and these trends increase with the significant wave height. We observe that wind speeds from ASAR and ASCAT have a close resemblance which helps us extrapolate our findings. The synergy between the two technologies can be further exploited to improve wind speed retrievals. Future scatterometer missions, such as the next MeTop, will operate with wider range of incidence angles (including lower angles) to increase their coverage together, have higher spatial resolution, and obtain measurements closer to the coasts. In these cases high resolution SAR data can aide in the understanding of the radar response.**

***Index Terms*—ocean winds, synthetic aperture radar, scatterometer, sea-state bias, backscatter**

I. Introduction

ACTIVE microwave radars aboard space-borne satellites are sensitive to the ocean surface roughness. The primary application of measured ocean surface roughness is the estimate of near surface oceanic wind speeds at 10 m elevation (hereafter U10). Typical errors on wind vectors obtained from various missions such as QuikSCAT [1], the Advanced SCATterometer (ASCAT) [2], and RapidSCAT (RSCAT) [3] are 1 m/s for speed, less than 20° for directions and satisfying mission requirements leading to other applications. In particular, remotely sensed oceanic wind speeds improved our ability to forecast [4] and understand the climate [5], heat fluxes [6], [7], and ocean mixing [8].

Geophysical model functions (GMF) which relate the normalized radar cross section (σ_0) to U10 have continuously improved their performance to measure U10 [9], [10]. However, despite the success of the scatterometer missions and GMFs, improvements are certainly possible. In particular, areas with atmospheric instability, strong ocean surface currents, extreme conditions with both high wind speed and large waves or low wind speeds remain challenging [11], [12], [13]. Thanks to the new capabilities of recent C-band SAR missions and the increasing quantity SAR acquisitions, new opportunities such as the use of cross-polarization or the Doppler centroid anomaly have been proposed to improve wind speed retrieval in extreme winds [14], [15] or decrease the weight of an a-priori solution for wind direction [16]. This yielded significant changes in the strategy for next generation of MetOp scatterometer [17] to include cross-polarization [18] and proposition of new concepts to take benefit of Doppler [19].

Besides the effects from atmospheric stability and surface currents, the measured radar signal varies with the local slope or tilt of the sea surface which is related to the wave steepness. In practice it is difficult to describe the tilt effect because ocean waves are random and the local wind field is often uncoupled with wave field due to remotely generated swell and rapidly turning winds. Furthermore contemporary satellite technologies do not directly measure the wave steepness. Therefore we hypothesize that the tilt of the ocean surface influences σ_0 and the resulting U10 retrieval. This has been observed by [20] using the scatterometer aboard ERS2. They found that U10 dependencies to sea state reduce with increasing incidence angle from 25 to 55°. For radars with large incidence angles like SeaWinds on QuikSCAT (θ=52°), U10 errors have minimal effect from the sea state [1]. At the lower end of the regime, between nadir and 20°, the impact of waves on the σ_0 has been documented for Ku- and Ka-Band based on TRMM [21], [22] and GPM missions [23]. Consequently, for ($\theta \in$20-30), we also expect waves to have an impact on C-Band σ_0 and U10. In this study we extend the analysis of [20] to the Advanced Synthetic Aperture Radar (ASAR) aboard Envisat and ASCAT aboard MetOp-A and describe the wave impacts as a function of sea state. To date, these effects have not been addressed in sufficient detail which is the purpose of our study.

Both the ASAR and ASCAT sensors use electromagnetic waves in the C-Band and operate in VV-polarization. ASAR has a near fixed incident angle of 23° while ASCAT has a range of incidence angles from 25 to 64° and uses three antennas. [15] found estimates of U10 and σ_0 from SAR and scatterometers are consistent; therefore, using these platforms enables us to specifically address the incidence angle dependence of the wind retrievals. ASAR's lower near fixed incidence angle in "Wave Mode" (acquisition mode operated over oceans for swell retrieval), allows us to study the tilt effects with a global coverage. To directly address the sea state impact within σ_0 and U10 we use in-situ buoys from the National Data Buoy Center (NDBC). In addition, we benefit

J. Stopa is the corresponding author justin.stopa@ifremer.fr. J. Stopa, A. Mouche, and B. Chapron are with Laboratoire d'Océanographie Spatiale, Ifremer, Plouzané, France.

F. Collard is with the Ocean Data Lab, Plouzané, France.

Manuscript submitted June 1, 2016 to JSTARS special issue: New Challenges and Opportunities in Scatterometry

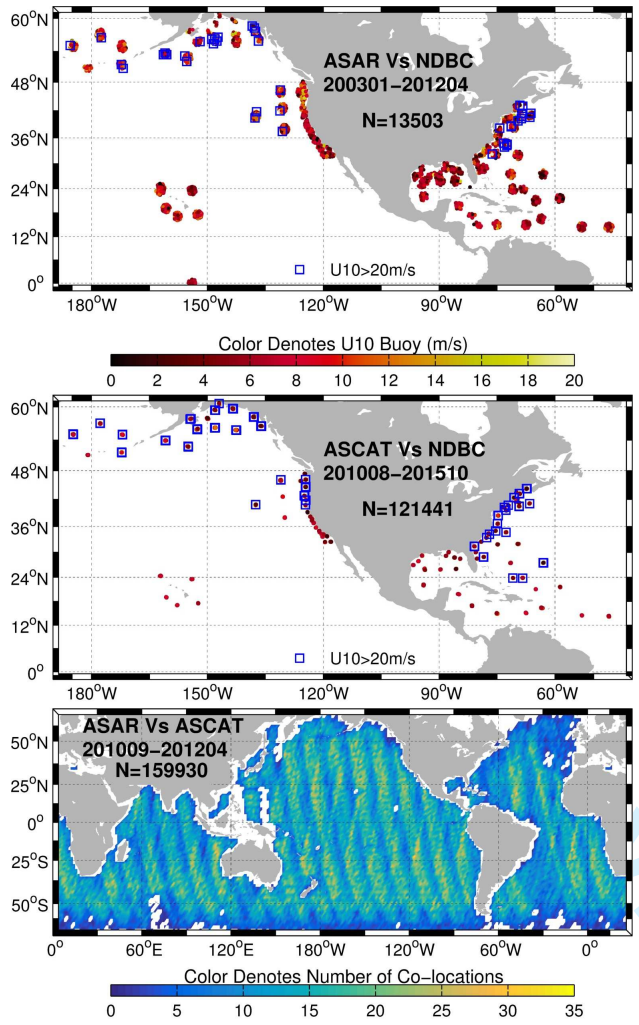

Fig. 1. Co-locations between ASAR and NDBC (top), ASCAT and NDBC (middle), and ASAR and ASCAT (bottom). The top two panels give an indication of the wind speed and the bottom panels shows the number of co-locations in 2° bins.

from the favorable orbits of ASCAT and ASAR to build a match-up database for 2010-2012. This enables us to extend our SAR analysis to higher incidence angles.

The paper is organized as follows. The datasets are described in section 2 with specific subsections that describe SAR, scatterometer, buoy observations, and wind data from reanalysis. In section 3, we inter-compare the ASAR and ASCAT wind retrievals to the observed buoys wind speeds. Our discussion and conclusions follow in sections 4 and 5.

II. Datasets

This study is possible since multiple observing satellites are in orbit during an overlapping period and fly overhead NDBC buoys numerous times. The resulting crossover datasets are sufficiently large and create statistically meaningful results. The following subsections describe the datasets and our methodology.

A. Advanced synthetic aperture radar on Envisat

SARs make use of their platform displacement and the phase of their emitted signal to capture high resolution ocean scenes. Sea surface displacements introduce Doppler shifts which distort the phases of returned radar signal and create constructive or destructive effects. By taking advantage of the constructive components, ocean waves can be measured [24], [25]. The destructive effects create an apparent blurring or distortion along the satellite path known as the azimuth cutoff [26], [27]. Here we focus on U10 computed from the mean backscatter estimated from the SAR imagettes.

The European Space Agency (ESA) Envisat satellite was equipped with the the advanced synthetic aperture radar sensor (ASAR) and in orbit for nearly a decade (2002-2012). We use data recorded from the "Wave Mode" which has the spatial resolution and footprint size of 9x6 m and 10x7 km respectively. ASAR uses microwaves in the C-band using VV polarization with an incidence angle of approximately 23°. During the 10 year mission several altitude changes occurred to help offset the decaying strength of the emitted electromagnetic signals. Therefore σ_0 was calibrated in time removing errors associated with Envisat's shifts in orbit and sensor power decay. Our analysis is based on observations when the normalized variance of the imagette is less than 1.5 to exclude anomalous objects and slicks contained in the ocean scenes. Otherwise all SAR imagettes are systematically processed to derive the σ_0 from the backscatter intensity.

The GMF of CMOD5N by [28] is used to estimate U10 from ASAR at 10x7 km resolution under neutral atmospheric stability and represents a 8-10 minute average. CMOD5N is valid for C-band radars with incidence angles from 18 to 60°. The algorithm uses σ_0, incidence angle (θ), and wind direction relative to the satellite track (ϕ) as input. It was developed to minimize U10 errors globally. U10 computed using CMOD5N for extreme winds in Hurricane Ivan showed improved performance over its predecessor, CMOD4 [29]. In all cases we use the wind direction (ϕ) derived from ASCAT or measured by the buoy as input to CMOD5N.

B. Advanced scatterometer on MetOp-A

Scatterometers are radars that actively pulse microwaves and record a backscatter mostly driven by the small-scales (centimeters at C-Band) roughnesses from the sea surface. As the wind blows over the ocean surface, it generates surface roughness (capillary-waves) aligned with the wind and directly related to the backscatter. The wind speeds and directions are thus retrieved from the analysis of measured backscatter. The wind direction is determined by multiple view angles but often have a 180° ambiguity [2]. In this study we use the data from the ASCAT instrument aboard MetOp-A, which uses the C-band (5.2 GHz with 5.7 cm wavelengths). Microwaves from the C-band are less influenced by water vapor in the atmosphere and consequently perform better than Ku-band radars when rain is present [30]. This mission covers approximately 97% of the oceans every 48 hrs.

ASCAT has three antennas on either side of the instrument orientated at 45°, 90°, and 135° relative to the satellite

heading. The incidence angles vary between 25-53° and 34-64° for the mid and outer beams respectively. The sensors on each side resolve a swath of 500 km with a separation of 360 km below the satellite. The surface resolution is approximately 12.5 km for each wind estimate. Comparisons to independent buoy observations show ASCAT has root mean square wind speed and direction errors less than 1.8 m/s and 20° [31], [10]. To be consistent with ASAR, we use CMOD5N of [28] to estimate U10 for ASCAT.

C. Buoy observations from the National Data Buoy Network

Buoy data are essential in-situ observations used to assess the wind speeds estimated from the ASAR and ASCAT. We use quality controlled measurements from the National Data Buoy Center (NDBC) network. The buoys are located in various climates near Hawaii, Alaska, Northeast Pacific, Gulf of Mexico, and the Northwest Atlantic (Figure 1). Most buoy anemometers are 5 m from the ocean surface; therefore the wind speed is converted to 10 m elevation assuming a neutrally stable boundary layer. Most buoys provide information about the environment like the atmospheric pressure, atmospheric temperature, and sea surface temperature. Wind speeds are computed using a 10-minute average and only buoys equipped with concurrent wind and wave observations are used in the analysis.

The buoys accurately resolve wave energy up to 0.04 Hz [32]. For frequencies larger than 0.04 Hz we assume the wave energy cascades with the parametric shape of f^{-5}. The power -5 is created by the balance between wave breaking and growth and is applicable for a large range of sea states [33]. The contribution from the higher frequencies plays a role in the azimuth cutoff [27]. The significant wave height (H_s) is calculated from wave spectrum $E(f)$:

$$H_s = 4\sqrt{M_{(p=0)}} \tag{1}$$

where M_p represents the p-th moment of the wave spectrum

$$M_p = \int_0^\infty (2\pi f)^p E(f) df. \tag{2}$$

H_s is proportional to the zeroth moment of the wave spectrum and gives a magnitude of the sea state mixing all wave frequencies. However, it does not provide detailed wave information that might be more important for remote sensing applications. Therefore, we analyze other wave parameters including the swell wave height (H_{ss}), average wave period ($Tm02$), azimuth cutoff (λ_c), mean squared acceleration (MSA), and wave age (WA) are defined as:

$$H_{ss} = 4\sqrt{\int_0^{0.08} E(f) df} \tag{3}$$

$$Tm02 = \sqrt{\frac{M_0}{M_2}} \tag{4}$$

$$\lambda_c = \pi \frac{R}{V} \sqrt{M_2} \tag{5}$$

$$MSA = M_4 \tag{6}$$

$$WA = C_p / U10 \tag{7}$$

where R/V is the range to platform velocity (120 s for Envisat), and C_p is the group velocity of the dominate waves.

D. The Climate Forecast System Reanalysis CFSR

Wind information from the Climate Forecast System Reanalysis (CFSR) provides a complementary source of information. The NCEP CFSR provides wind speeds from 1979-present [34], [35]. The important advancements of CFSR with respect to its predecessors Reanalysis I and II consist of coupling between the ocean, atmosphere, land surface, and sea ice model, increased horizontal and vertical resolution in the atmospheric model, and assimilation of satellite radiances. The atmospheric model has a resolution of approximately 0.3° (37 km) and now 0.2° (22 km) and assimilates data in three dimensions. CFSR assimilates scatterometer wind data so it is not an entirely independent data source. CFSR is available hourly and U10 is linearly interpolated in time and space to match the satellite observations.

E. Co-locations

This study is based on the co-locations between ASAR and the NDBC buoys, ASAR and ASCAT, and ASCAT and the NDBC buoys. ASAR/NDBC are limited to 100 km in space (dx<100 km) and equate to time differences less than 30 minutes. The ASAR/ASCAT and NDBC/ASCAT match-ups are limited to 13 km in space and 30 minutes in time. Figure 1 shows the co-locations for all datasets. In total there are approximately 1.3×10^4, 1.2×10^5 and 1.6×10^5 data pairs for ASAR/NDBC, ASCAT/NDBC, and ASAR/ASCAT covering a large range of sea state conditions. In the ASAR/NDBC and ASCAT/NDBC datasets, most wind speeds range from 1 to 20 m/s with only 44 and 131 instances larger than 20 m/s. The ASAR/ASCAT dataset provides comprehensive coverage with the majority of the 2° grid cells having larger than 20 data pairs. This dataset has 297 (0.1%) events with U10 larger than 20 m/s. Therefore the majority of our results are valid within the range 1 to 20 m/s.

III. ASAR AND ASCAT WIND RETRIEVAL COMPARISON

It is our goal to assess U10 errors and investigate the differences in the co-located datasets. Figure 2 presents scatterplots of the three datasets with standard error metrics given in the top left corners. We calibrated σ_0 from ASAR to obtain zero U10 bias with the buoys when dx<30 km (top left panel). Notice that the error dispersion is roughly 1.5 m/s about the least-squared linear regression line (dashed lines). The top right panel shows ASAR/NDBC data when dx<100 km. By relaxing the distance requirement, the error dispersion increases to 3 m/s; but the overall error metrics are similar. ASAR has a small U10 bias of +20 cm/s and when U10 is larger than 15 m/s. The bottom left panel shows the ASAR/ASCAT comparison. The linear regression line is nearly one-to-one demonstrating a close resemblance of the C-band satellite datasets and the dispersion is roughly 1 m/s about the one-to-one line. Similar to the buoy comparison,

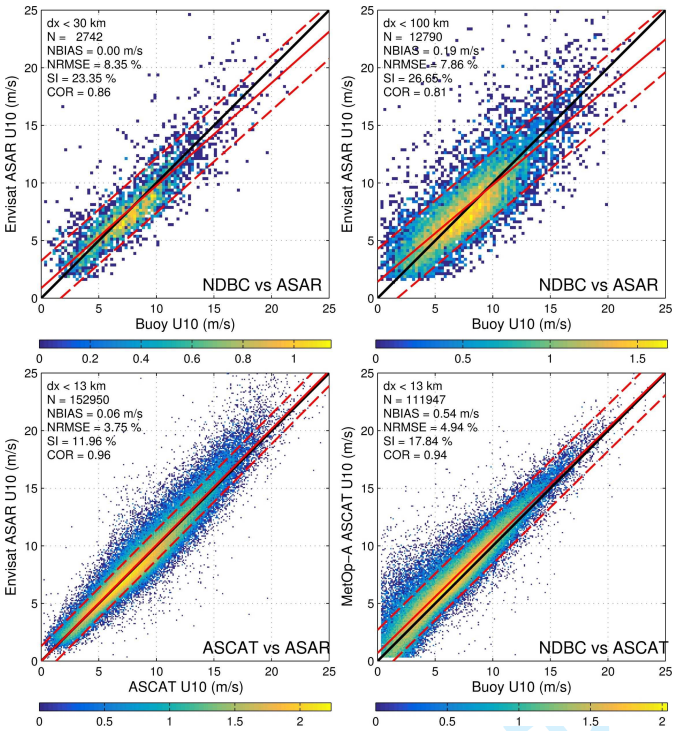

Fig. 2. Wind speed comparisons between NDBC and ASAR when distances are less than 30 km (top left), NDBC and ASAR (top right), ASCAT and ASAR (bottom left), and NDBC and ASCAT (bottom right). The red line represents the least squared regression and the dashed red lines contain 95% of the data points. The colors represent the number of observations on a logarithmic scale (log10(N)) using 0.25 m/s and 0.1 m/s bins for the top and bottom panels respectively.

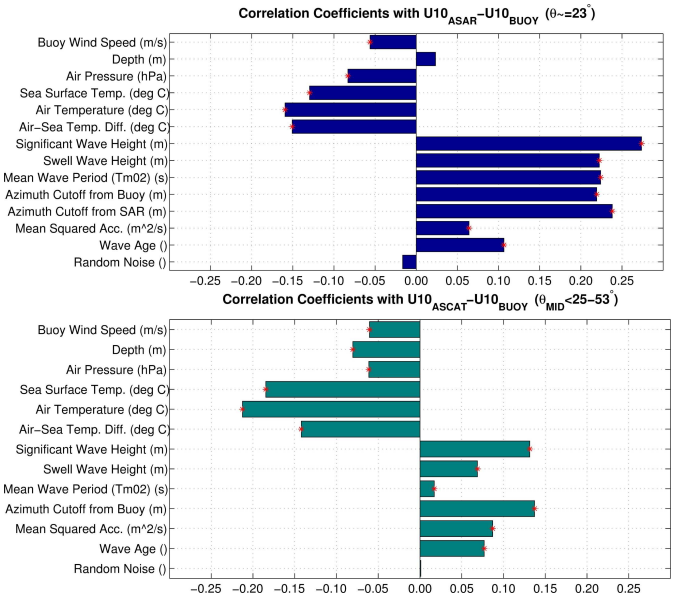

Fig. 3. Correlation coefficient between U10 errors ($U10_{ASAR}-U10_{NDBC}$) (top) $U10_{ASCAT} - U10_{NDBC}$) (bottom) and various in-situ buoy observations. A red "*" denotes statistical significance at the 95% level.

ASAR overestimates the largest wind speeds. Results obtained with NDBC/ASCAT co-locations are given in the bottom right panel. These datasets are highly correlated and have a small bias of 0.5 m/s that is apparent for the most common wind speeds of 6 to 8 m/s. When the wind speed is low (< 5 m/s), there is larger variability in the biases. Some of this variability can be attributed to random errors in the buoy wind speeds [36]. In addition, the wind variability introduces errors if not considered [37]. Also notice that wind speeds larger than 15 m/s follow the observations much better than ASAR. In summary, the wind speed errors from ASAR and ASCAT obtained with CMOD5N are comparable to the buoy observations but with significant error dispersion. The error dispersion is larger for winds derived with ASAR. The following deals with the analysis of this error dispersion.

We explore the relationship of the residuals by computing correlation coefficients with geophysical parameters measured by in-situ buoys. The results are given in Figure 3 for both ASAR (top) and ASCAT (bottom). There is a negative correlation between ASAR U10 residuals and the buoy wind speed. This can be explained by the top panels of Figure 2 where there is an overestimation when U10 is less than 5 m/s and the trend decreases with increasing wind speed. There is no relationship with the buoy depth suggesting that the ASAR provides consistent observations in both deep and shallow water environments, which is important for practical ocean engineering applications. In the bottom panel, as for ASAR, the ASCAT residuals have a negative correlation with U10 consistent with the small negative linear regression line in the bottom panel of Figure 2. In this case there is negative bias with the buoy depth. As the buoy depth decreases the U10 errors increase suggesting larger errors for shallow water locations and hence nearshore environments. The atmospheric stability effects seen by the correlation coefficients from air pressure, sea surface temperature, air temperature, and air-sea temperature difference all have a negative correlation with the residuals from both ASAR and ASCAT. Therefore low atmospheric pressures with colder temperatures, which are located in higher latitudes, tend to have larger errors. The correlation coefficients of the atmospheric stability variables are more pronounced in the ASCAT data than in the ASAR data. C-band radars are insensitive to changes in sea surface salinity, therefore we did not consider their effects. Only over major river plumes will sea surface salinity affect the radar cross section [38].

All the wave parameters have positive relationships with the residuals. The H_s and azimuth cutoff have the largest correlation coefficients for the wave quantities in both datasets. Notice that the magnitudes of the correlation coefficients are larger for ASAR compared to ASCAT. It should be noted that the overall mean radar cross section is conserved after the SAR processing. Accordingly, the mean $\sigma 0$ should be comparable for ASCAT and ASAR at a given incidence angle [15]. In addition, U10, H_s, and the azimuth cutoff are all inter-related making it difficult to separate their dependencies [39], [26]. In the ASCAT data, the correlation coefficients for $Tm02$ are reduced compared to the other wave parameters. In both cases the wave age, and indicator of swell, has reduced correlations coefficients in relation to the H_s. H_s mixes all wave scales and results in the strongest relationship with the U10 residuals. This parameter is strongly related to U10 itself

and less intuitive of the physical processes than other wave parameters. Here we use all of the ASCAT data where the mid beam incidence angle is $25-53^{\circ}$ while ASAR is near fixed at 23°. The radar sensitivity to the ocean surface depends on the incidence angle, thus the sea state impact is expected to vary with incidence angle.

To further explore the dependence between ASCAT residuals with incidence angle we compute the correlation coefficients for each wind vector cell. The results are displayed in the Figure 4 with the x-axis representing the approximate incidence angle of the mid-beam. To avoid statistical errors, each bin has the same number samples (2000) that are randomly chosen from the entire population. The wind retrieval algorithm takes into account the radiometric performance, which is worse for higher incidence angles. However the loss of radiometric resolution at high incidence angles is compensated by the fact that the sea surface roughness is more sensitive to changes in near surface winds. At lower incidence angles the wind speed has a larger negative correlation with the U10 residuals and creates a significant relationship. The correlation with depth (not shown) is nearly zero at low incidence angles and has increasing negative correlation coefficients as the incidence angle increases and is consistent with the ASAR results that have a slight positive correlation when $\theta = 23^{\circ}$. Buoy depth can be used as a proxy for distance to shore, therefore shallow water regions with large incidence angles have higher U10 errors. The air temperature has a negative correlation for all incidence angles and there is a larger influence at higher incidence angles. This is an expected result for C-band radars with VV polarization since Bragg scattering enhances the centimeter-scale ocean roughness at higher incidence angles. The correlation coefficients with H_s and H_{ss} in the top center and right panels show that the sea state dependence decays with increasing incidence angle. This relationship is more pronounced in the swell wave heights. The average wave period has correlation coefficients less than 0.15 but has a significant negative trend that decreases with increasing incidence angles. The wave age shows a clear relationship with the incidence angle. In summary, the ASCAT U10 residuals and incidence angle dependence based on the given sea state parameter vary in magnitude. The atmospheric stability strongly influences the errors and is more pronounced at higher incidence angles. The results consistently show that the swells, with larger wave ages, which are less dependent on high frequency motions, have a stronger relationship with the U10 residual at low incidence angles.

To further document the sea state impact on ASAR winds we compute least squared U10 linear regression lines for various wave height increments using ASAR (dx<30 km) in Figure 5. It is common to have taller wave heights coupled with stronger wind speeds and the precision of the buoy observations could be affected. To avoid this issue, we use U10 from CFSR to represent an independent data source (left panel). At low wind speeds there is an overestimation for all sea states, otherwise the influence from the waves is minimal within CFSR and the linear regression lines are within close proximity. This is not the case for the ASAR comparison shown in the right panel. There is a clear sea

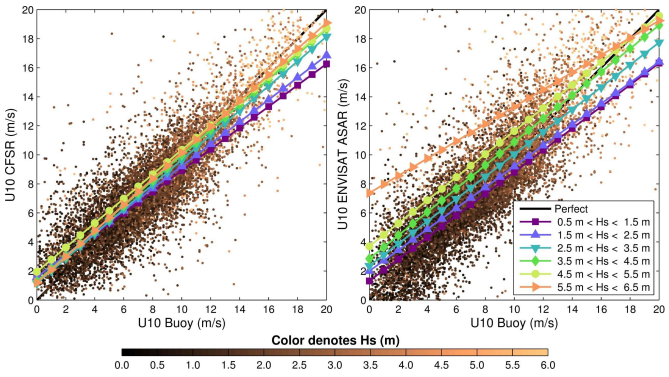

Fig. 5. Least squared linear regression between wind speeds: NDBC vs CFSR (left) and NDBC vs ASAR (right) as a function of H_s. Each linear regression line represents a range of significant wave heights and the colors denote H_s.

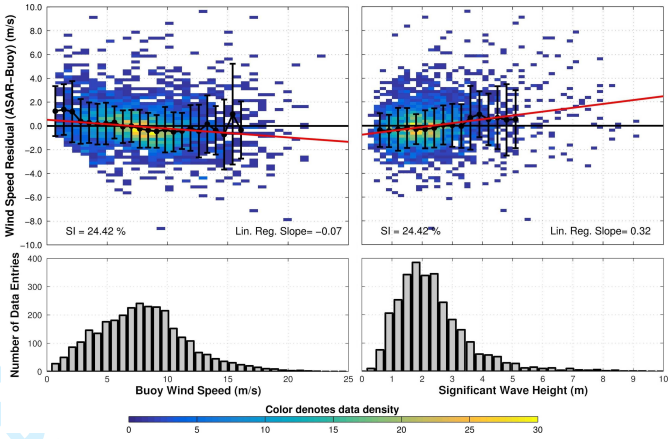

Fig. 6. Wind speed residuals ($U10_{ASAR} - U10_{buoy}$) as a function of buoy U10 (left) and H_s (right). The error bars represent 1 standard deviation about the average (black dots) and the red line represents the least square linear regression. The colors in the top panel denote data density and the bottom panels display the histograms with 0.75 m/s and 0.25 m bins respectively.

state dependence in ASAR using these triple co-locations. The U10 errors increase with H_s and this explains some of the error dispersion we observed in Figure 2. We must emphasize that these linear regressions depict average conditions and not instantaneous errors, which might be larger and are displayed in the background scatter plots.

To complement Figure 5, Figure 6 illustrates the ASAR U10 residuals (dx<30 km) as a function of U10 and H_s. The left panel shows that larger U10 errors occur at low and high wind speeds; however, the overall slope of the least squares linear regression line is negligible. The negative slope is caused by the wind speeds less than 3 m/s, where there is an average bias of 1.5 m/s. These errors are expected to be related to the presence of swell or poorly contrasted images. Notice that wind speeds larger than 10 m/s have increased variability and biases. The right panel shows a distinct relationship between the U10 residuals and the sea state through H_s. This relationship demonstrates that as the H_s increases the U10 residuals increase proportionally. In conclusion, the U10 residuals in the ASAR dataset have the strongest relationship with the sea state compared to the wind speed itself.

The relationship between σ_0, U10, and H_s is explored using

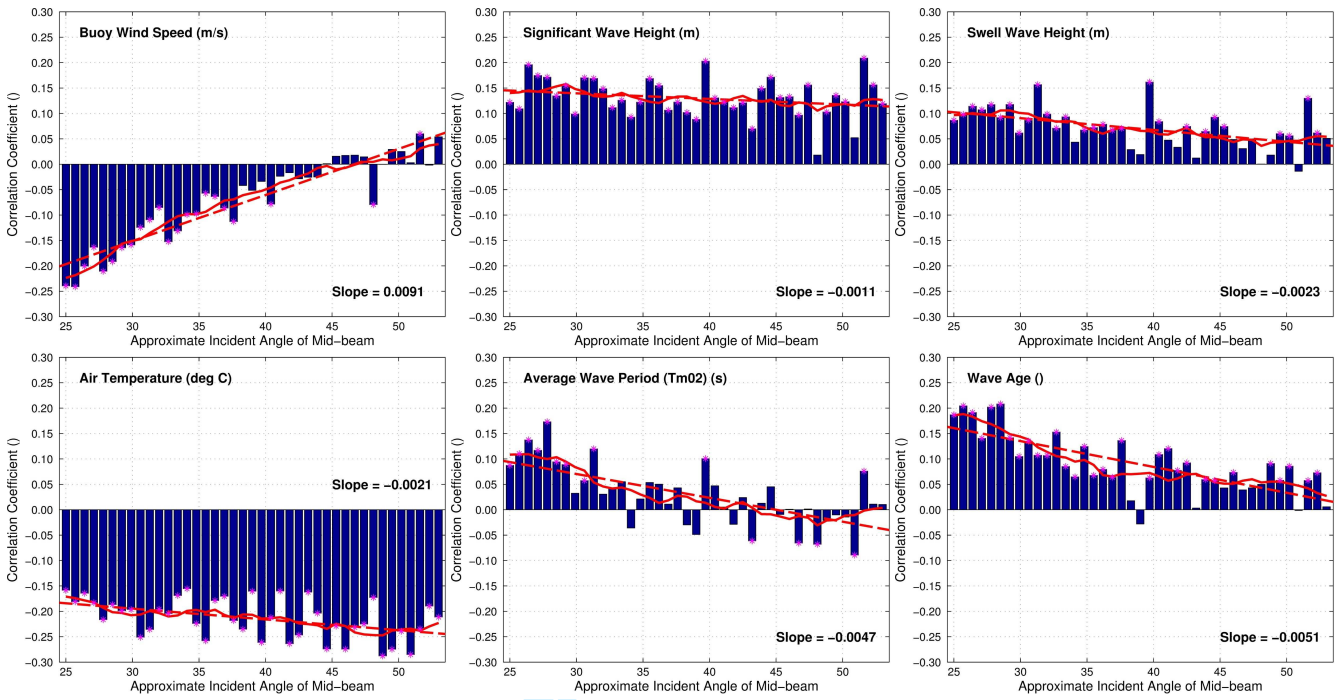

Fig. 4. Correlation coefficients between U10 residuals ($U10_{ASCAT} - U10_{buoy}$) and in-situ buoy observations: U10 (top left), significant wave height (top center), swell wave height (top right), mean squared acceleration (bottom left), average wave period (bottom center), and wave age (bottom right) as a function of incidence angle.

the ASAR/NDBC dataset. To help explain the impact of wind and waves on σ_0 we develop GMFs using neural networks to relate U10 to σ_0 ($\sigma_0 = F_1(U10)$) and then U10 and H_s to σ_0 ($\sigma_0 = F_2(U10, H_s)$). We create GMFs using a multilayer perceptron (MLP) with back propagation and segment the data into equal halves for training and validation [40]. To directly assess the U10 variability with the sea state we remove the effects from the wind direction by limiting the directions to small directional bandwidths for cross-wind ($\phi \in (80°, 100°)$) and up-wind ($\phi \in (-10°, 10°)$). The results are given in Figure 7 for the buoy observations (left), F_1 (center), and F_2 (right).

Buoy observations in the top left panel show that in cross-wind conditions when the wind speed is small (<5 m/s), σ_0 has a large variance. The backscattered intensity appears to saturate at -4 dB. The H_s (colors) explains some of the variations in U10 denoted by the H_s gradient that increases with U10. $F_1(U10)$ given in the top center panel shows the general trend that σ_0 increases with U10, but cannot explain the variance of the observations. The top right panel shows $F_2(U10, H_s)$, which captures some of the σ_0 variability. However, this function is not able to explain the small σ_0 (<-10 dB) and it is expected the function will overestimate σ_0. The bottom panels explore the up-wind conditions. Buoy observations in the bottom left panel show a similar relationship as the cross-wind conditions but the saturation level is much higher and σ_0 increases beyond -4 dB. $F_1(U10)$ in the bottom center panel matches the buoy curve but cannot explain the variability as well as $F_2(U10, H_s)$. This demonstration supports that the sea state influences the radar cross section and consequently the resulting wind speed retrievals.

IV. Discussion

The high number of co-locations between the buoys, Envisat/ASAR, and MetOp-A/ASCAT allowed a detailed description of the U10 errors derived from the ASAR and ASCAT sensors. CMOD5N is found to be a robust estimator of U10 and both ASAR and ASCAT match the in-situ buoy observations well. However, large error dispersion remains, most notably in the ASAR/NDBC dataset. The comparison of U10 residuals with in-situ observations including sea state parameters and atmospheric stability variables show that both have small but measurable impacts. The atmospheric stability and sea state are often interrelated and swell has been documented to affect the lower atmosphere [41], [42]. The ASAR errors are strongly related to the sea state conditions shown by the correlation coefficients with U10 errors and various wave parameters including the wave age and swell wave height. The U10 sea state dependence is included in σ_0 shown by the GMFs developed in Figure 7.

In the case of ASCAT the sea state impact on U10 is less pronounced. This is because the ASCAT wind vectors are derived from the combination of three antennas while ASAR has only one. The procedure of merging of the three σ_0's obtained from different azimuth look angles and incidence angles mitigates the sea state impacts because the tilt modulation is azimuth angle dependent. This explain why these errors are often overlooked. However, we still observe that the ASCAT U10 residuals have stronger correlations with significant wave height from swell and wave age for lower incidence angles in agreement with [20]. The analysis in Figure 4 consistently shows that swells are expected to influence the U10 residuals supporting our hypothesis that the tilting effect from remote

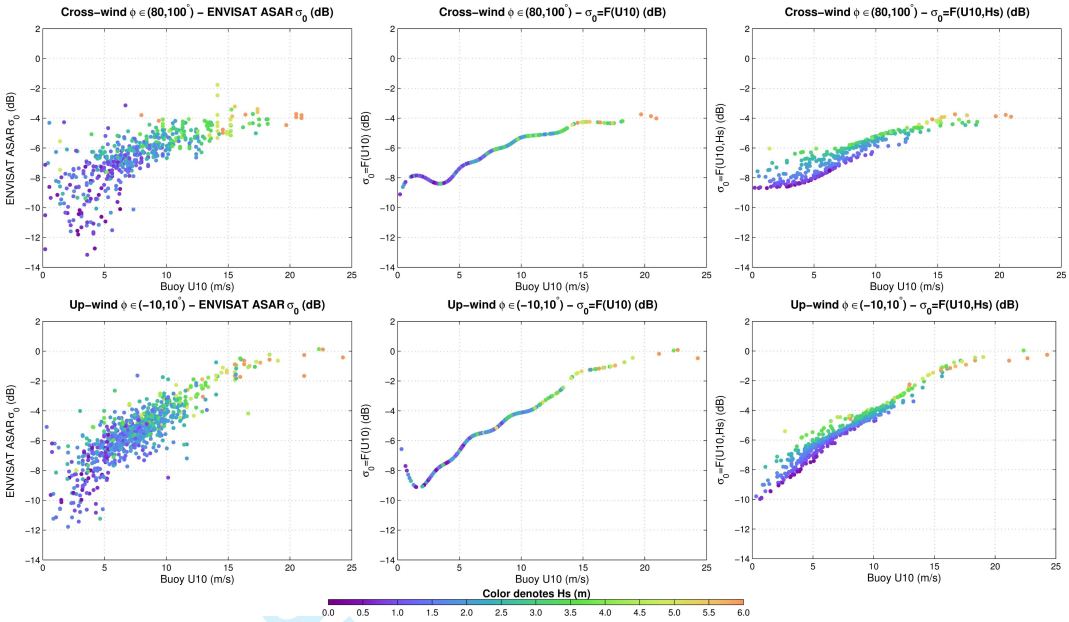

Fig. 7. Relationship between U10 Buoy, H_s (color), and $sigma_0$ from ASAR (left), predicted using a neutral network using ϕ,U10 as input (center), and predicted using a neutral network using ϕ,U10,H_s as input (right) to cross-wind (top) and up-wind (bottom) conditions.

swells can modify the σ_0. We expect the impact of sea state to be more important on σ_0 before the σ_0's are merged and comparable to the ASAR results for low incidence angles. This could be verified from ASCAT's σ_0 from the Level-1 product instead of using U10.

EUMETSAT is planning to launch a scatterometer aboard MetOp-SGA/B in 2021/2 that will operate with lower incidence angles ($\theta_{MID} = 20°$) to extend the spatial coverage by reducing the nadir gap. Based on our results we expect larger sea state effects on the wind speed retrievals at these lower incidence angles and further research will be needed to thoroughly assess this impact. An interesting aspect of this mission is the possible use of cross-polarization to improve the wind retrieval in extreme wind conditions. Extremes winds are often coupled with large values of H_s and the impact of waves on σ_0 is very relevant. Our analysis mostly focused on moderate sea states and it is expected that the sea state impact on σ_0 is enhanced at larger significant wave heights ($H_s > 8m$) as Figures 5 and 6 suggest.

When the incidence angles, emitted electromagnetic frequency, azimuth look angle, and resolution are equivalent the SAR and scatterometer backscatter should behave the same. This is supported by the close match between the sensors in Figure 2. SAR's high spatial resolution can be used to provide a reference for scatterometers as higher resolution products are being developed [43], [44]. SAR technology can aide in the interpretation of the spatial variability associated with the observed backscatter as well as validation of scatterometer measurements in the coastal areas. Even older missions like ERS2, which was equipped with both a scatterometer and SAR, may provide insights to the expected backscattered responses by comparing both sensors. Furthermore, the sea state dependency in the SAR could be corrected using the derived wave properties. Since SAR has high resolution and captures concurrent wave information it is possible to obtain higher U10 accuracy. With the increased data availability from the Sentinel-1 A and B missions, SAR data could provide a sufficiently large data source of U10 to train GMFs for scatterometer applications.

V. Conclusion

As we seek new methods to improve our ability to measure oceanic winds, it becomes increasingly important to accurately measure secondary response, such as sea tilt. From theory and observations we know that the measured backscattered response of sensors with smaller incidence angles are more influenced by the slope of the sea surface. The tilt is directly related to the presence of waves and our results demonstrate that the largest errors from ASAR are related to sea-state parameters. The same pattern is found in ASCAT but the effect is reduced since three radar cross sections from different incidence angles and azimuth look angles are used to estimate a single U10. By including sea state parameters in a GMF for SAR, we could improve U10 retrievals. We conclude that at smaller incidence angles ($< 40°$) the sea-state impacts U10 measurements if not directly addressed. While our results were limited to ENVISAT ASAR and MetOp-A ASCAT, it is expected that U10 errors exist in other satellite datasets. Future studies should consider tilt effects from the sea state to improve U10 estimates.

Acknowledgment

JS was supported by LabexMER through grant ANR-10-LABX-19 with additional support from the Research Laboratory in Hydrodynamics, Energetics and Atmospheric Environment (LHEEA) at Ecole Centrale, Nantes. All datasets are publicly available: NCEP's CFSR (rda.ucar.edu), Envisat ASAR (globwave.ifremer.fr), ASCAT (eumetsat.int), and the NDBC buoy data (www.nodc.noaa.gov/BUOY/).

REFERENCES

[1] N. Ebuchi, H. C. Graber, and M. J. Caruso, "Evaluation of wind vectors observed by quikscat/seawinds using ocean buoy data," *Journal of Atmospheric and Oceanic Technology*, vol. 19, no. 12, pp. 2049–2062, Dec 2002. [Online]. Available: http://dx.doi.org/10.1175/1520-0426(2002)019<2049:EOWVOB>2.0.CO;2

[2] B. A. Stoffelen and D. Anderson, "Ambiguity removal and assimilation of scatterometer data," *Quarterly Journal of the Royal Meteorological Society*, vol. 123, no. 538, pp. 491–518, Jan 1997. [Online]. Available: http://dx.doi.org/10.1002/qj.49712353812

[3] A. C. Paget, D. G. Long, and N. M. Madsen, "Rapidscat diurnal cycles over land," *IEEE Transactions on Geoscience and Remote Sensing*, vol. 54, no. 6, pp. 3336–3344, Jun 2016. [Online]. Available: http://dx.doi.org/10.1109/TGRS.2016.2515022

[4] L. Bi, J. A. Jung, M. C. Morgan, and J. F. Le Marshall, "Assessment of assimilating ascat surface wind retrievals in the ncep global data assimilation system," *Monthly Weather Review*, vol. 139, no. 11, pp. 3405–3421, Nov 2011. [Online]. Available: http://dx.doi.org/10.1175/2011MWR3391.1

[5] F. J. Wentz, L. Ricciardulli, K. Hilburn, and C. Mears, "How much more rain will global warming bring?" *Science*, vol. 317, no. 5835, pp. 233–235, Jul 2007. [Online]. Available: http://dx.doi.org/10.1126/science.1140746

[6] A. Bentamy, S. A. Grodsky, K. Katsaros, A. M. Mestas-Nunez, B. Blanke, and F. Desbiolles, "Improvement in air-sea flux estimates derived from satellite observations," *International Journal of Remote Sensing*, vol. 34, no. 14, pp. 5243–5261, Jul 2013. [Online]. Available: http://dx.doi.org/10.1080/01431161.2013.787502

[7] G. P. King, J. Vogelzang, and A. Stoffelen, "Second-order structure function analysis of scatterometer winds over the tropical pacific," *Journal of Geophysical Research: Oceans*, vol. 120, no. 1, pp. 362–383, Jan 2015. [Online]. Available: http://dx.doi.org/10.1002/2014JC009992

[8] T. Lee, O. Wang, W. Tang, and W. T. Liu, "Wind stress measurements from the quikscat-seawinds scatterometer tandem mission and the impact on an ocean model," *Journal of Geophysical Research*, vol. 113, no. C12, Dec 2008. [Online]. Available: http://dx.doi.org/10.1029/2008JC004855

[9] F. J. Wentz and D. K. Smith, "A model function for the ocean-normalized radar cross section at 14 GHz derived from nscat observations," *Journal of Geophysical Research: Oceans*, vol. 104, no. C5, pp. 11 499–11 514, May 1999. [Online]. Available: http://dx.doi.org/10.1029/98JC02148

[10] J. Verspeek, A. Stoffelen, M. Portabella, H. Bonekamp, C. Anderson, and J. Saldana, "Validation and calibration of ascat using cmod5.n," *IEEE Transactions on Geoscience and Remote Sensing*, vol. 48, no. 1, pp. 386–395, Jan 2010. [Online]. Available: http://dx.doi.org/10.1109/TGRS.2009.2027896

[11] R. N. Hoffman and J.-F. Louis, "The influence of atmospheric stratification on scatterometer winds," *Journal of Geophysical Research*, vol. 95, no. C6, p. 9723, 1990. [Online]. Available: http://dx.doi.org/10.1029/JC095iC06p09723

[12] A. M. Plagge, D. Vandemark, and B. Chapron, "Examining the impact of surface currents on satellite scatterometer and altimeter ocean winds," *Journal of Atmospheric and Oceanic Technology*, vol. 29, no. 12, pp. 1776–1793, Dec 2012. [Online]. Available: http://dx.doi.org/10.1175/JTECH-D-12-00017.1

[13] A. Plagge, J. B. Edson, and D. Vandemark, "In situ and satellite evaluation of air-sea flux variation near ocean temperature gradients," *J. Climate*, vol. 29, no. 4, pp. 1583–1602, Feb 2016. [Online]. Available: http://dx.doi.org/10.1175/JCLI-D-15-0489.1

[14] P. A. Hwang, A. Stoffelen, G.-J. van Zadelhoff, W. Perrie, B. Zhang, H. Li, and H. Shen, "Cross-polarization geophysical model function for c-band radar backscattering from the ocean surface and wind speed retrieval," *Journal of Geophysical Research: Oceans*, vol. 120, no. 2, pp. 893–909, Feb 2015. [Online]. Available: http://dx.doi.org/10.1002/2014JC010439

[15] A. Mouche and B. Chapron, "Global c-band envisat, RADarsat-2 and sentinel-1 Sar measurements in copolarization and cross-polarization," *Journal of Geophysical Research: Oceans*, vol. 120, no. 11, pp. 7195–7207, Nov 2015. [Online]. Available: http://dx.doi.org/10.1002/2015JC011149

[16] A. A. Mouche, F. Collard, B. Chapron, K.-F. Dagestad, G. Guitton, J. A. Johannessen, V. Kerbaol, and M. W. Hansen, "On the use of doppler shift for sea surface wind retrieval from sar," *IEEE Transactions on Geoscience and Remote Sensing*, vol. 50, no. 7, pp. 2901–2909, Jul 2012. [Online]. Available: http://dx.doi.org/10.1109/TGRS.2011.2174998

[17] C.-C. Lin, M. Betto, M. Belmonte Rivas, A. Stoffelen, and J. de Kloe, "Eps-sg windscatterometer concept tradeoffs and wind retrieval performance assessment," *IEEE Transactions on Geoscience and Remote Sensing*, vol. 50, no. 7, pp. 2458–2472, Jul 2012. [Online]. Available: http://dx.doi.org/10.1109/TGRS.2011.2180393

[18] F. Fois, P. Hoogeboom, F. Le Chevalier, and A. Stoffelen, "Future ocean scatterometry: On the use of cross-polar scattering to observe very high winds," *IEEE Transactions on Geoscience and Remote Sensing*, vol. 53, no. 9, pp. 5009–5020, Sep 2015. [Online]. Available: http://dx.doi.org/10.1109/TGRS.2015.2416203

[19] F. Fois, P. Hoogeboom, F. Le Chevalier, A. Stoffelen, and A. Mouche, "Dopscat: A mission concept for simultaneous measurements of marine winds and surface currents," *Journal of Geophysical Research: Oceans*, vol. 120, no. 12, pp. 7857–7879, Dec 2015. [Online]. Available: http://dx.doi.org/10.1002/2015JC011011

[20] Y. Quilfen, B. Chapron, F. Collard, and D. Vandemark, "Relationship between ers scatterometer measurement and integrated wind and wave parameters," *Journal of Atmospheric and Oceanic Technology*, vol. 21, no. 2, pp. 368–373, Feb 2004. [Online]. Available: http://dx.doi.org/10.1175/1520-0426(2004)021<0368:RBESMA>2.0.CO;2

[21] N. Tran, B. Chapron, and D. Vandemark, "Effect of long waves on ku-band ocean radar backscatter at low incidence angles using trmm and altimeter data," *IEEE Geosci. Remote Sensing Lett.*, vol. 4, no. 4, pp. 542–546, Oct 2007. [Online]. Available: http://dx.doi.org/10.1109/LGRS.2007.896329

[22] X. Chu, Y. He, and G. Chen, "The relationship between radar backscatter cross section and ocean wave parameters at low incidence angles," *2009 IEEE International Geoscience and Remote Sensing Symposium*, 2009. [Online]. Available: http://dx.doi.org/10.1109/IGARSS.2009.5417637

[23] F. Nouguier, B. Chapron, A. Mouche, N. Rascle, and D. Vandemark, "Analysis of dual-frequency ocean backscatter measurements at ku- and ka-band using near-nadir incidence gpm radar data." *IEEE Geosci. Remote Sensing Lett.*, 2016.

[24] B. Chapron, H. Johnsen, and R. Garello, "Wave and wind retrieval from sar images of the ocean," *Annales Des Telecommunications*, vol. 36, no. 11, pp. 682–699, 2001. [Online]. Available: http://link.springer.com/article/10.1007/BF02995562

[25] F. Collard, F. Ardhuin, and B. Chapron, "Extraction of coastal ocean wave fields from sar images," *IEEE J. Oceanic Eng.*, vol. 30, no. 3, pp. 526–533, Jul 2005. [Online]. Available: http://dx.doi.org/10.1109/JOE.2005.857503

[26] V. Kerbaol, B. Chapron, and P. W. Vachon, "Analysis of ers-1/2 synthetic aperture radar wave mode imagettes," *Journal of Geophysical Research: Oceans*, vol. 103, no. C4, pp. 7833–7846, Apr 1998. [Online]. Available: http://dx.doi.org/10.1029/97JC01579

[27] J. E. Stopa, F. Ardhuin, B. Chapron, and F. Collard, "Estimating wave orbital velocity through the azimuth cutoff from space-borne satellites," *Journal of Geophysical Research: Oceans*, vol. 120, no. 11, pp. 7616–7634, Nov 2015. [Online]. Available: http://dx.doi.org/10.1002/2015JC011275

[28] H. Hersbach, A. Stoffelen, and S. de Haan, "An improved c-band scatterometer ocean geophysical model function: Cmod5," *Journal of Geophysical Research*, vol. 112, no. C3, Mar 2007. [Online]. Available: http://dx.doi.org/10.1029/2006JC003743

[29] J. Horstmann, D. R. Thompson, F. Monaldo, S. Iris, and H. C. Graber, "Can synthetic aperture radars be used to estimate hurricane force winds?" *Geophysical Research Letters*, vol. 32, no. 22, 2005. [Online]. Available: http://dx.doi.org/10.1029/2005GL023992

[30] D. E. Fernandez, J. R. Carswell, S. Frasier, P. S. Chang, P. G. Black, and F. D. Marks, "Dual-polarized c- and ku-band ocean backscatter response to hurricane-force winds," *Journal of Geophysical Research*, vol. 111, no. C8, 2006. [Online]. Available: http://dx.doi.org/10.1029/2005JC003048

[31] A. Bentamy, D. Croize-Fillon, and C. Perigaud, "Characterization of ascat measurements based on buoy and quikscat wind vector observations," *Ocean Science*, vol. 4, no. 4, pp. 265–274, Dec 2008. [Online]. Available: http://dx.doi.org/10.5194/os-4-265-2008

[32] D. Vandemark, B. Chapron, T. Elfouhaily, and J. W. Campbell, "Impact of high-frequency waves on the ocean altimeter range bias," *Journal of Geophysical Research*, vol. 110, no. C11, 2005. [Online]. Available: http://dx.doi.org/10.1029/2005JC002979

[33] W. J. Pierson and L. Moskowitz, "A proposed spectral form for fully developed wind seas based on the similarity theory of s. a. kitaigorodskii," *Journal of Geophysical Research*, vol. 69, no. 24, pp. 5181–5190, Dec 1964. [Online]. Available: http://dx.doi.org/10.1029/JZ069i024p05181

[34] S. Saha, S. Moorthi, H.-L. Pan, X. Wu, J. Wang, S. Nadiga, P. Tripp, R. Kistler, J. Woollen, D. Behringer, and et al., "The ncep climate forecast system reanalysis," *Bulletin of the American Meteorological Society*, vol. 91, no. 8, pp. 1015–1057, Aug 2010. [Online]. Available: http://dx.doi.org/10.1175/2010BAMS3001.1

[35] S. Saha, S. Moorthi, X. Wu, J. Wang, S. Nadiga, P. Tripp, D. Behringer, Y.-T. Hou, H.-y. Chuang, M. Iredell, and et al., "The ncep climate forecast system version 2," *J. Climate*, vol. 27, no. 6, p. 2185?2208, Mar 2014. [Online]. Available: http://dx.doi.org/10.1175/JCLI-D-12-00823.1

[36] Y. Quilfen, B. Chapron, and D. Vandemark, "The ers scatterometer wind measurement accuracy: Evidence of seasonal and regional biases," *Journal of Atmospheric and Oceanic Technology*, vol. 18, no. 10, p. 16841697, Oct 2001. [Online]. Available: http://dx.doi.org/10.1175/1520-0426(2001)018<1684:TESWMA>2.0.CO;2

[37] K. Shankaranarayanan and M. A. Donelan, "A probabilistic approach to scatterometer model function verification," *Journal of Geophysical Research: Oceans*, vol. 106, no. C9, p. 1996919990, Sep 2001. [Online]. Available: http://dx.doi.org/10.1029/1999JC000189

[38] N. Reul, S. Saux-Picart, B. Chapron, D. Vandemark, J. Tournadre, and J. Salisbury, "Demonstration of ocean surface salinity microwave measurements from space using amsr-e data over the amazon plume," *Geophys. Res. Lett.*, vol. 36, no. L13607, 2009.

[39] K. Hasselmann and S. Hasselmann, "On the nonlinear mapping of an ocean wave spectrum into a synthetic aperture radar image spectrum and its inversion," *Journal of Geophysical Research*, vol. 96, no. C6, p. 10713, 1991. [Online]. Available: http://dx.doi.org/10.1029/91JC00302

[40] J. Gourrion, D. Vandemark, S. Bailey, B. Chapron, G. P. Gommenginger, P. G. Challenor, and M. A. Srokosz, "A two-parameter wind speed algorithm for ku-band altimeters," *Journal of Atmospheric and Oceanic Technology*, vol. 19, no. 12, pp. 2030–2048, Dec 2002. [Online]. Available: http://dx.doi.org/10.1175/1520-0426(2002)019<2030:ATPWSA>2.0.CO;2

[41] V. N. Kudryavtsev and V. K. Makin, "Impact of swell on the marine atmospheric boundary layer," *Journal of Physical Oceanography*, vol. 34, no. 4, pp. 934–949, Apr 2004. [Online]. Available: http://dx.doi.org/10.1175/1520-0485(2004)034<0934:IOSOTM>2.0.CO;2

[42] U. Hogstrom, A. Smedman, E. Sahle, W. M. Drennan, K. K. Kahma, H. Pettersson, and F. Zhang, "The atmospheric boundary layer during swell: A field study and interpretation of the turbulent kinetic energy budget for high wave ages," *Journal of the Atmospheric Sciences*, vol. 66, no. 9, pp. 2764–2779, Sep 2009. [Online]. Available: http://dx.doi.org/10.1175/2009JAS2973.1

[43] A. Verhoef, M. Portabella, and A. Stoffelen, "High-resolution ascat scatterometer winds near the coast," *IEEE Transactions on Geoscience and Remote Sensing*, vol. 50, no. 7, pp. 2481–2487, Jul 2012. [Online]. Available: http://dx.doi.org/10.1109/TGRS.2011.2175001

[44] R. D. Lindsley, C. Anderson, J. Figa-Saldana, and D. G. Long, "A parameterized ascat measurement spatial response function," *IEEE Transactions on Geoscience and Remote Sensing*, pp. 1–10, 2016. [Online]. Available: http://dx.doi.org/10.1109/TGRS.2016.2544835